

Copyright © 1997 Elsevier Science Ltd

Int. J. Rock Mech. & Min. Sci. Vol. 34, No. 3-4, 1997 ISSN 0148-9062

To cite this paper: *Int. J. Rock Mech. & Min. Sci.* **34:3-4**, Paper No. 024

DAMAGE ACCUMULATION DURING TRIAXIAL CREEP OF DARLEY DALE SANDSTONE FROM PORE VOLUMOMETRY AND ACOUSTIC EMISSION

P. BAUD¹; P. G. MEREDITH²

¹ *Ecole et Observatoire de Physique du Globe de Strasbourg, Laboratoire de Physique des Matériaux, 5 rue René Descartes, 67084 Strasbourg Cedex, France*

² *Rock and Ice Physics Laboratory, Department of Geological Sciences, University College London, Gower Street, London W61E 6BT, UK*

ABSTRACT

We performed triaxial creep tests on water-saturated samples of Darley Dale sandstone to investigate the effect of pressure on the process of time-dependent brittle deformation under all-round compression. Axial strain, acoustic emission (AE) output and pore volume change were monitored continuously during each test. We observed the three classical creep regimes (primary, steady-state and tertiary). The level of applied differential stress has a crucial effect on the creep rate and on the time-to-failure; from 30 minutes at 90% of the short-term strength to almost one day at 80%. For the experiments performed at the lower levels of stress, the duration of the primary creep phase increases, while the acoustic emission level during the steady-state phase decreases dramatically. The variations of axial strain and differential pore-fluid volume are more regular when the tests are conducted at stresses closer to the strength of the material. AE measurements suggest that the final stage of the deformation occurs for similar levels of cumulative events and cumulative AE energy, regardless of stress level. The same comment can be made for the pore-fluid volumetry results. This suggests that the final stage that leads to failure occurs for almost the same level of damage in all samples.

Copyright © 1997 Elsevier Science Ltd

KEYWORDS

Triaxial Testing • Reservoir Rocks • Creep • Acoustic Emission • Pore-fluid Volume • Damage

INTRODUCTION

Aqueous pore fluids exert a great influence on brittle rock deformation in a number of ways. First, there is the mechanical role of pressurised pore fluids that weakens and embrittles rocks, and is usually expressed in terms of the *law of effective stress* (e.g. Paterson 1978; Sammonds *et al.* 1995). Secondly, there is the chemical influence of pore fluids that allows cracks to propagate even at very low stresses, through such mechanisms as stress corrosion (Atkinson, Meredith 1987), and leads to time- and rate-dependent deformation and strength. The dependence of stress corrosion on pressure is still not well understood, since many previous studies (e.g. Meredith, Atkinson 1983; Atkinson, Meredith 1981) have been for purely tensile fracture under ambient conditions. To date, there has been no direct evidence of

the influence of pressure on subcritical crack growth and its consequent effect on damage evolution under compression, although indirect evidence from static fatigue tests (Kranz 1979, 1980) indicates that the application of pressure significantly influences fatigue strength and may inhibit stress corrosion. Several aspects of this problem require investigation. Firstly, the crack damage states under compression are very different from those under tension, so that the average stress intensity of crack arrays depends on stress state; and secondly, the stress corrosion process will depend on pressure because the chemical activity of the pore fluid is affected by pressure.

We have investigated this problem experimentally, and here we report results from a series of laboratory triaxial-creep (static fatigue) experiments performed on water-saturated samples of Darley Dale sandstone. The tests were conducted under all-round compression, under stress regimes that are characteristic of reservoir conditions, up to stresses close to the short-term failure stress. We study the creep behaviour in relation to applied stress, and since accumulated cracking is commonly treated as a stable damage variable, we quantify the evolution of damage volume in the rock using both pore-fluid volumetry and acoustic emission statistics. Although macroscopically stable and quasi-static, damage evolves by increments of crack growth that are dynamic enough to produce acoustic emissions.

EXPERIMENTAL DETAILS

Triaxial deformation apparatus

The triaxial-deformation experiments were undertaken in the Rock & Ice Physics Laboratory at University College London. Right-cylindrical jacketed samples of water-saturated rock (100 mm long \times 40 mm diameter) were deformed in a triaxial cell that can simulate pressures up to 400 MPa using silicone oil as the pressure medium. For the experiments reported here, the confining pressure was controlled to within about 1% by an external servo-controlled pressure-intensifier.

The differential load is applied by an external servo-hydraulic actuator via a pressure-balanced ram assembly, and operating under either load or displacement-rate control. Axial stress and strain are determined to within about 1% after allowance for seal friction and elastic shortening of the loading train.

Pore volumetry measurements

The specimen pedestal was used to conduct high-pressure tubing from both ends of the sample to an external servo-controlled pore-fluid pressure intensifier and volumeter (Read *et al.* 1989). The volumeter essentially comprises a long, small-diameter piston moving within two close coupled pressure chambers at different operating pressures. Movement is controlled in the low-pressure chamber by an electronic servocontrol unit, with the selectable feedback signal being provided by a pressure transducer connected to the high-pressure chamber. A displacement transducer coupled to the piston allows continuous monitoring of changes in sample pore-fluid volume during experiments conducted at constant pore-fluid pressure (drained conditions).

Acoustic emission measurements

A lead-zirconate-titanate (PZT) piezoelectric acoustic emission (AE) transducer was located close to the sample in the hollow lower ram. The PZT has a high response band in the frequency range 100 kHz to 1 MHz. Signals from the transducer were amplified using a close-coupled 40 dB low-noise pre-amplifier, and then passed to a PAC Locan AT acoustic emission monitor for recording and analysis (see Meredith *et al.* 1990). The analyser was programmed to apply a further amplification of 40 dB and to accept data

above a 38 dB threshold value. The level of the threshold value was set such that extraneous background noise was eliminated from the recorded data. The number of AE events (wave packets produced by individual cracking events in the rock), and their amplitude and energy, were all logged as a function of time.

Sample material and preparation

All samples were of Darley Dale sandstone, a poorly sorted, well-indurated felspathic sandstone from the North of England with a grain size ranging from 0.08 mm to 0.8 mm. The cementing material is predominantly silicious. This sandstone was chosen for its relative homogeneity. All the samples were cored from a single block, and their total porosity varied between 12% and 14%. The pore size distribution, measured by mercury porosimetry, is essentially unimodal with a mean pore diameter of 10 μm , but with significant microporosity (Read *et al.* 1995). Samples were oven dried at 70°C for 48 h after coring, before being finally dried in a vacuum of 10^{-3} Torr for several hours prior to vacuum saturation with distilled water.

Test conditions

In all experiments, the confining pressure was controlled at 75 MPa, and the pore-fluid pressure (distilled water) was controlled at 45 MPa. These pressure conditions can be found in the crust at depths in the range 3 to 5 km. The confining pressure was applied first, and after setting the pore-fluid pressure, the samples were loaded at a constant axial strain rate up to the desired level of axial stress. From that point, axial stress was maintained constant while axial strain, acoustic emission output and pore volume change were monitored continuously (i.e. at 30s sampling intervals). The total number of tests performed was 15, but for reasons of space we report only results from selected tests here.

EXPERIMENTAL RESULTS

Results from short-term strength and stress level tests

The short-term strength (maximum differential stress) of the material under these particular experimental conditions was determined from constant strain rate tests run to failure at a strain rate of $4 \times 10^{-6} \text{ s}^{-1}$. The mean value of the peak stress was found to be 160.5 MPa, with a maximum variation between samples of about 5%. Figure 1 (a, b, c) shows the change in axial stress, axial strain, pore-fluid volume (differential pore fluid volume, ΔP_v), and acoustic emission output (AE energy rate and cumulative AE energy) recorded during one of these tests. The pore-fluid volume decreases during the early stage of loading due to compaction. Preexisting radial cracks and some pores are closed by the application of axial stress, and the consequence is an effective decrease in damage volume and expulsion of pore-fluid from the sample. No acoustic emission activity is recorded during this period.

As axial stress is increased further, some new axial cracks are nucleated, and this produces both a stagnation in the pore-fluid volume change and the onset of acoustic emission activity. At about two-thirds of the peak stress, the damage volume (as measured by ΔP_v) starts to increase, and the rate of pore-volume increase during dilatancy is much higher than the rate of pore volume decrease during compaction. The dilatancy is accompanied by a significant increase in the acoustic emission activity.

In the final stage of the test (from around peak stress), the AE energy rate, increases dramatically as the result of the crack interaction and coalescence that leads to macroscopic failure. The differential

pore-fluid volume increases by about 0.4 cm^3 during the last 20% of the test, representing two-thirds of the total volume increase. For all samples, failure occurs by shear faulting at approximately 30° to the direction of the maximum principal stress.

We have also carried out a number of incremental stress tests to estimate the times-to-failure for different levels of constant differential stress. As with previous studies, these experiments demonstrated one of the classical features of the creep process; namely that the time-to-failure increases dramatically with decrease in stress level. For example, we found that at stress levels below 80% of the short-term strength, no significant creep could be measured, even over a period of more than 3 days. The pore-volume and axial strain remained essentially constant, with the total strain change being less than 0.1%. Clearly, the 80% level does not strictly represent the lower bound for creep, and given enough time this stress level would produce very slow creep and eventual failure of the sample. However, in order not to introduce extra problems associated with running ultra-long experiments, we have taken the 80% of peak stress level as the lower bound for our study.

Figure 1 (d, e, f) illustrates the importance of the level of differential stress on the creep process. Starting at 80% of the peak stress, we increased the axial stress in small steps to about 90%, leaving the stress applied for a short time at each level. The effect of changing the stress level can clearly be seen in all the parameters measured. At first, the axial strain increases so slowly that it is only possible to see the evolution of damage by small increases in the pore-fluid volume and the cumulative AE energy. However, with each incremental increase in stress level, the slope of the strain/time curve increases significantly. In turn, this suggests a significantly reduced time-to-failure for each increase in stress level. Around 90% of the peak stress, the strain rate becomes exceptionally high, and this is accompanied by a very high AE energy rate. This represents a stress level at which crack interaction is already important, and the sample failed in less than one more hour. Further tests have shown that creep deformation is uncontrollable at stress levels above 90% of the peak stress. The strain is exponential, and no steady-state creep occurs. This behaviour is beyond the range that we wish to study, and we have therefore taken a stress level of 90% of peak stress as the upper bound for our study.

Results from creep experiments

Figure 2 shows the results from three creep experiments conducted at 90%, 85% and 80% of the peak stress. The loading system was switched from strain-rate control to load control when the desired level of axial stress was reached. During the creep phase, fluctuations in the axial load were less than 1%. For all tests, we found very similar patterns in the evolution of axial strain, differential pore-fluid volume and cumulative AE energy. For example, the minimum in the differential pore-fluid volume was always found to be around -0.1 cm^3 . This enabled an independent check that the rock had been properly saturated.

Figure 2 also shows the three creep regimes that have been described in previous studies (e.g. Gangi 1983, Cristescu 1989). The creep starts with a primary phase during which the strain rate is initially high but decreases with time. If the stress level is high enough (i.e. above 80% of peak stress), the primary phase is followed by the main phase of secondary (steady-state) creep. Time-dependent cracking plays the major role during this phase, and produces AE events primarily of small amplitude (and energy). Finally, all experiments end with a period of tertiary creep characterised by an exponential increase in strain rate leading to macroscopic failure.

The level of stress has a crucial effect on the creep rate and *a fortiori* on the time-to-failure; from 30 minutes at 90% of the peak stress (146 MPa), to about four hours at 85% (138 MPa), and to almost a day at 80% (130 MPa). In fact, the duration of all three creep phases increases with decrease in stress level. For example, the duration of the primary creep phase increases from only a few minutes for sample PAD9 (90%), to about 30 minutes for sample PAD13 (85%), and almost 3 hours for sample PAD6 (80%). The primary creep rate decreases relatively rapidly to reach a stable value that marks the onset of secondary creep. However, because the initial creep rate is high, the contribution of primary creep to the total damage accumulation in the samples is strongly dependent on its duration. The contribution of primary creep to damage volume appears virtually insignificant for sample PAD9, whereas it contributes a volume increase of about 0.05 cm³ for sample PAD6 (close to 50% of that accumulated during secondary creep in the same sample). Finally, at the boundary between primary creep and steady-state creep, all of the measured parameters have very similar values for all three experiments: axial strain is close to 1.2%; differential pore-fluid volume is close to zero; and cumulative AE energy is close to 1000.

The main phase of the experiment is the steady-state creep phase. Its duration increases from 26 min at 90% of the peak stress to about 20 h at 80%. The associated creep rates decrease with decreasing stress level from $7 \times 10^{-7} \text{ s}^{-1}$ for sample PAD9 (90%), to $8 \times 10^{-8} \text{ s}^{-1}$ for sample PAD13 (85%), and less than $3 \times 10^{-9} \text{ s}^{-1}$ for sample PAD6 (80%).

The increases in axial strain and differential pore-fluid volume appear more regular for the tests conducted at higher stresses, whereas at lower stress the creep appears to be a less continuous process with damage seeming to increase in steps of irregular length and amplitude. The differential pore-fluid volume increases are all between 0.05 and 0.10 cm³ during secondary creep, and the rate of AE activity is also uniformly low. For example, we found the same value of AE event rate of 3 events per minute for each of the three tests. As a consequence, the cumulative AE energy also increases slowly to reach a value close to 1500, just prior to the abrupt increase in creep rate that marks the onset of tertiary creep. Overall, these observations suggest that the changes from primary to secondary creep, and from secondary to tertiary creep, occur for essentially the same level of damage in all samples, regardless of stress level.

The final phase of tertiary creep is characterised by rapid increases in all the measured parameters. For samples PAD9 and PAD13, the creep rate increases exponentially before failure after 2 minutes and 15 minutes, respectively. For sample PAD6, tertiary creep starts with an abrupt increase in all the measured parameters. However, despite a jump in strain of the order of 0.1%, it still takes more than an hour for the sample to finally fail.

Despite the consistent behaviour of many of the samples we have tested, we have also been confronted by some problems of repeatability. An illustration of this problem is given in Figure 3, which shows results from a test on another sample (PAD11) conducted at 85% of the peak stress. The curves are very different from those shown on Figure 2 for sample PAD13 (85%). The total duration of the PAD11 test exceeded two days, while the PAD13 test lasted only about four hours. The main creep phase for PAD11 also exhibits different behaviour, with three successive intervals of steady-state creep before failure. The different mechanical behaviour is thought to be due to variability between samples in terms of porosity and initial damage state. For sample PAD11, the cumulative AE energy only reaches the value of about 1000 that marks the onset of secondary creep after about 5 hours, as against less than 1 hour for PAD13. This implies that it took much longer to accumulate the same level of damage in sample PAD11 than in sample PAD13. Furthermore, the differential pore-fluid volume at the start of secondary creep in PAD11

is abnormally high, which implies a different evolution of damage in this sample. We have seen that significant and controllable creep deformation in Darley Dale sandstone occurs only between 80% and 90% of the peak stress (an interval of 20 MPa). Relatively small variations in porosity and strength between samples can therefore potentially alter the creep behaviour dramatically, and result in either very rapid failure or a total absence of creep. This observation is linked directly to the process we are studying, and not to the experimental procedure.

CONCLUSIONS AND PERSPECTIVES

Our experimental results presented highlight some important characteristics of the time-dependent behaviour of rocks during static fatigue under all-round compression. We have shown that the creep rate and the time-to-failure are strongly correlated with the level of applied stress. However, the problem of repeatability suggests that stress level alone is not a rigorous indicator of the internal state of damage in rock samples. Variability between samples could lead to misinterpretation of results, because the same level of stress does not necessarily correspond to the same stage of damage evolution. Creep experiments can only strictly be repeatable if they use samples with exactly the same level of initial damage. However, the on-line parameters that we have used to quantify damage (cumulative AE energy, and differential pore-fluid volume) show very similar variations, and are consistent with the evolution of strain with time. Because AE statistics and pore-volumetry measure very different things, the very similarity of the curves suggests that these parameters track damage evolution in the samples very well. For example, they enable us to identify samples that are “under-damaged” or “over damaged” at a given level of stress. Where different samples exhibit similar changes in differential pore-fluid volume and cumulative AE energy at the onset of creep, we find almost exactly the same creep behaviour and time-to-failure. Our results also show that the state of damage at the onset of secondary creep is very similar in all the samples, regardless of stress level. The time-to-failure is then controlled by the rate of steady-state creep. Similarly, we find that the onset of tertiary creep occurs for an essentially constant level of damage, as estimated from pore volumetry and acoustic emission statistics. This could potentially provide a means for identifying the point at which the mechanical behaviour starts to be controlled by localisation of deformation in a damage zone that eventually evolves into a fault and leads to macroscopic failure.

AE event rates and energy rates have exhibited very similar trends throughout all of the creep experiments. Main, Sammonds, Meredith 1993 have proposed a model, based on experimentally derived acoustic emission data, that applies a modified Griffith failure criterion to predict the evolution of subcritical fractal damage compressive rock deformation. The model predicts stress corrosion indices for fracture under compression that are about an order of magnitude lower than those reported for simple tensile fracture. We will test this model systematically with the new data included in this paper.

FIGURES

Paper 024, Figure 1.

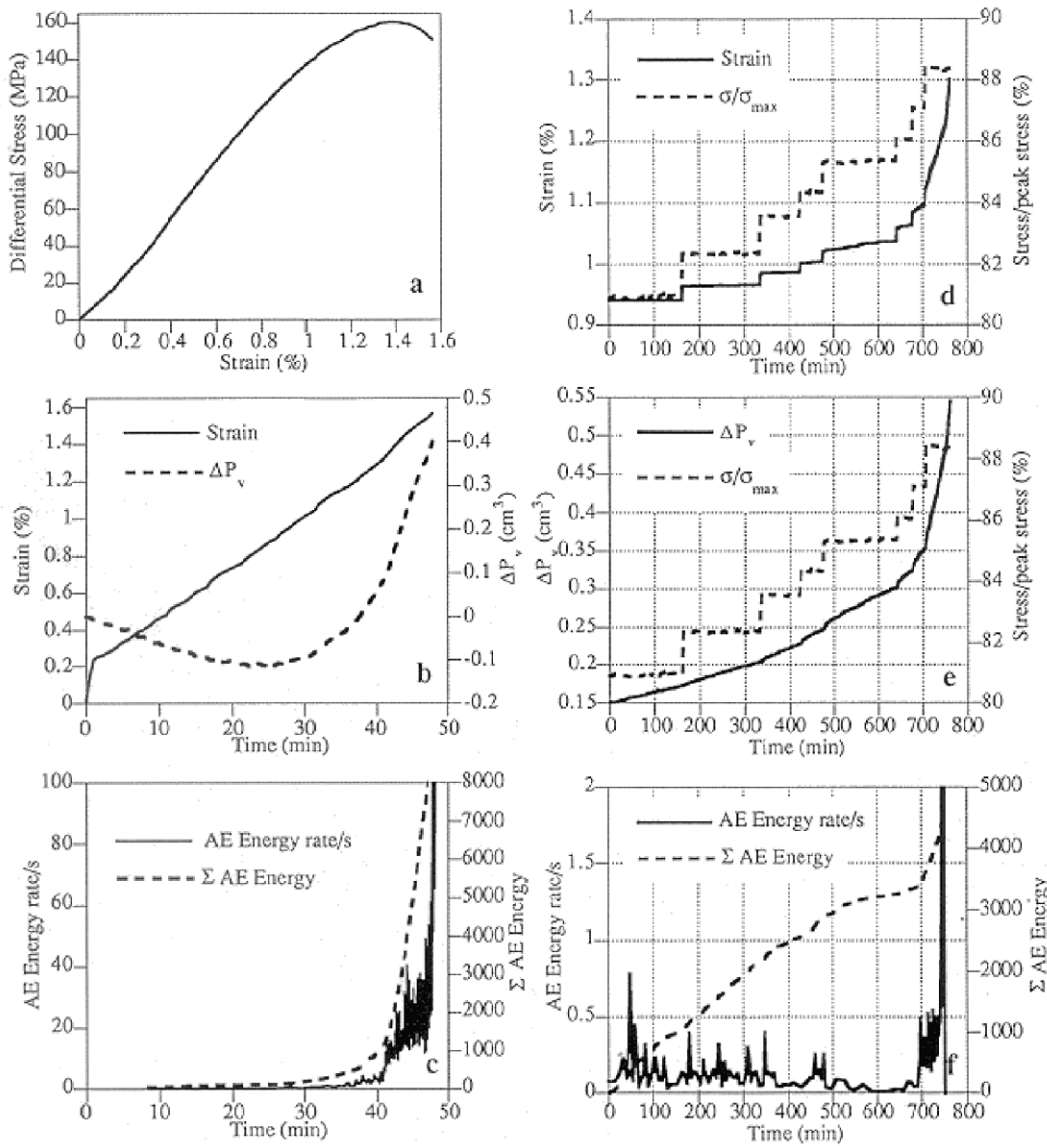


Figure 1. a to c: Constant strain rate test to failure (sample PAD4 : $\phi=13.97\%$). d to f: The axial stress is increased manually by steps from 80% to 90% of the peak stress (sample PAD10, $\phi=12.6\%$). a: Differential stress against strain, b: Strain and differential pore-fluid volume against time, c: Cumulative AE Energy against time, d: Strain and normalised differential stress against time, e: Differential pore-fluid volume and normalised stress against time, f: AE energy rate and cumulative AE energy against time.

Paper 024, Figure 2.

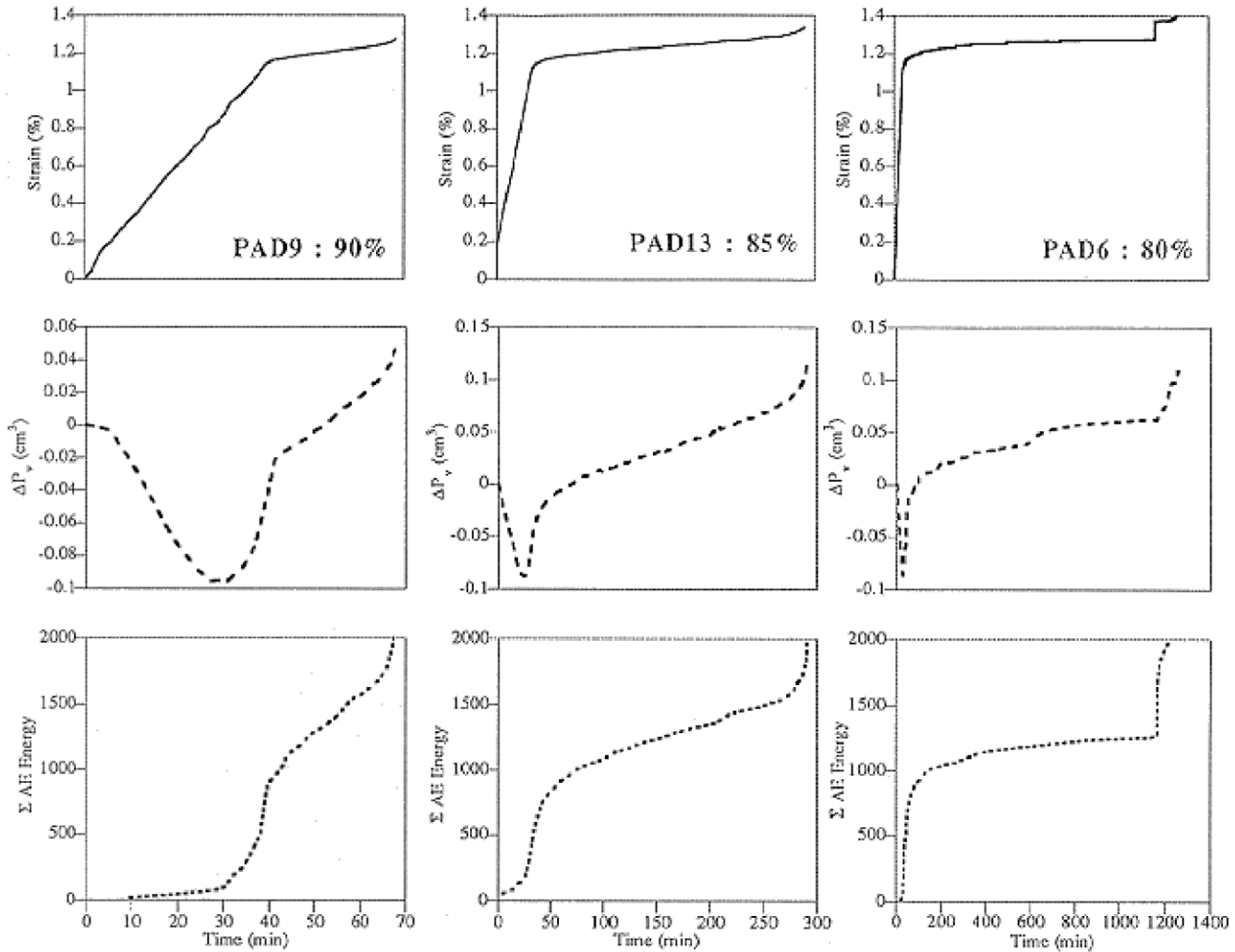


Figure 2. strain, differential pore-fluid volume and cumulative AE energy against time for three experiments.

- sample PAD9 ($\phi=12.75\%$), creep test at 90% of the peak stress
- sample PAD13 ($\phi=14.35\%$), creep test at 85% of the peak stress
- sample PAD6 ($\phi=14.26\%$), creep test at 80% of the peak stress

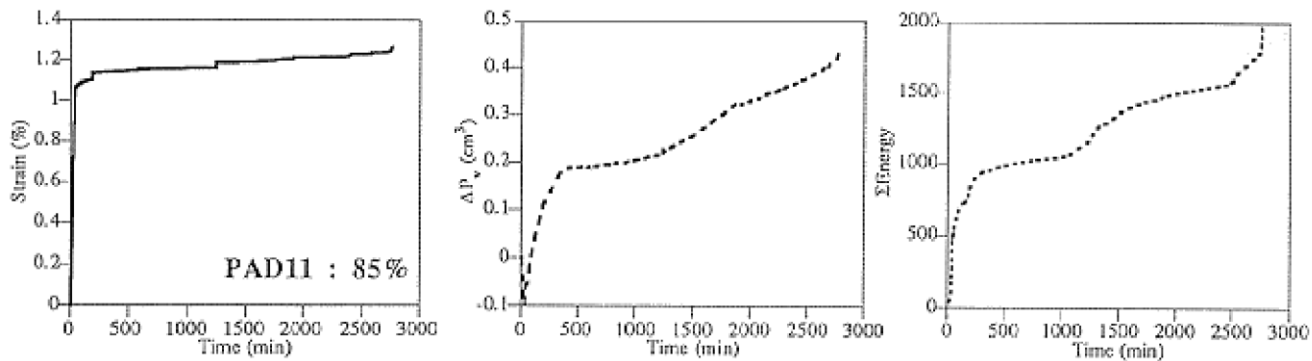
Paper 024, Figure 3.

Figure 3. strain, differential pore-fluid volume and cumulative AE energy against time for a creep test at 85% of the peak stress, sample PAD11 ($\phi=12.6\%$)

References**References**

- Atkinson B. K., Meredith P. G. 1981 Stress corrosion of quartz: a note on the influence of chemical environment. *Tectonophysics*, **77**, 1–11.
- Atkinson B. K., Meredith P. G. 1987. The theory of subcritical crack growth with applications to minerals and rocks. In *Fracture Mechanics of Rock*, Academic Press, London, 111–166.
- Cristescu N. 1989. *Rock Rheology*, Kluwer Academic Publishers, Dordrecht.
- Gangi A. F. 1983. Transient and steady-state deformation of synthetic rocksalt. *Tectonophysics*, **91**, 137–156.
- Kranz R. L. 1979. Crack growth and development during creep of Barre granite. *International Journal of Rock Mechanics and Mining Sciences*, **16**, 23–35.
- Kranz R. L. 1980. The effects of confining pressure and stress difference on static fatigue of granite. *J. Geophys. Res.*, **85**, 1854–1866.
- Main I. G., Sammonds P. R., Meredith P. G. 1993. Application of a modified Griffith criterion to the evolution of fractal damage during compressional rock failure. *Geophys. J. Int.*, **115**, 367–380.
- Meredith P. G., Atkinson B. K. 1983. Stress corrosion and acoustic emission during tensile crack propagation in Whin Sill dolerite and other basic rocks. *Geophys. J.R. Astron. Soc.*, **75**, 1–21.
- Meredith P. G., Main I. G., Jones C. 1990. Temporal variations in seismicity during quasi-static and dynamic rock failure. *Tectonophysics*, **175**, 249–268.
- Paterson M. S. 1978. *Experimental Rock Deformation - The Brittle Field*, Springer, Berlin.
- Read M. D., Meredith P. G., Murrell S. A. F. 1989. Permeability measurement techniques under hydrostatic and deviatoric stress conditions. In: *Rock at Great Depth (Eds: V. Maury & D. Fourmaintraux Vol 1)*, Balkema, Rotterdam, 211–218.

Read M. D., Ayling M. R., Meredith P. G., Murrell S. A. F. 1995. Microcracking during triaxial deformation of porous rocks monitored by changes in rock physical properties, II. Pore volumetry and acoustic emission measurements on water-saturated rocks. *Tectonophysics*, **245**, 223–235.

Sammonds P. R., Meredith P. G., Gomez J. B., Main I. G. 1995. The interaction between pore fluid pressure and crack damage evolution in rocks and rock structures modelled from acoustic emission data. *J. Acoustic Emission*, **13**, S21-S28.